Article

Template-Directed Synthesis of Photocatalyst-Encapsulating Metal-Organic Frameworks with Boosted Photocatalytic Activity

Xiaojie Yang, Tao Liang, Jiaxing Sun, Michael J. Zaworotko, Yao Chen, Peng Cheng, and Zhenjie Zhang

ACS Catal., **Just Accepted Manuscript** • DOI: 10.1021/acscatal.9b01783 • Publication Date (Web): 10 Jul 2019

Template-Directed Synthesis of Photocatalyst-Encapsulating Metal-Organic Frameworks with Boosted Photocatalytic Activity

Xiaojie Yang,[†, §] Tao Liang,[‡] Jiaxing Sun,[¶] Michael J. Zaworotko,[⊥] Yao Chen,[¶] Peng Cheng,[†, §,*] Zhenjie Zhang[†,¶,§,*]

[†] College of Chemistry, Nankai University, Tianjin 300071, China

[‡] Merck Center for Catalysis at Princeton University, Princeton, NJ 08544, USA

[¶] State Key Laboratory of Medicinal Chemical Biology, Nankai University, Tianjin 300071, China

[§] Key Laboratory of Advanced Energy Materials Chemistry, Ministry of Education, Nankai University, Tianjin 300071, China

[⊥] Department of Chemical Sciences, Bernal Institute, University of Limerick, Limerick V94T9PX, Republic of Ireland

Supporting Information Placeholder

ABSTRACT: In the past decade, the use of visible light to promote organic transformations has gained intense attention. In this study, we developed a template-directed synthesis method to use homogenous Ru and Ir photocatalysts as structure-directing templates and succeeded to prepare a series of photocatalyst-encapsulating metal-organic frameworks (photocatalyst@MOFs) with zeolite-like structures. The open channels and polyhedral cages of MOFs allowed effectively disperse the encapsulated photocatalysts and facilitated the transport of reactants and products, leading to boosted catalytic activity and good reusability toward important organic reactions such as aerobic oxidation reaction of benzyl halides and the cyclization of tertiary anilines and maleimides under visible light. Moreover, we also demonstrate the versatility and universality of our templating strategy. It not only can form MOFs which cannot be accessed by other synthesis methods, but also can encapsulate various commercially available homogeneous photocatalysts into MOFs. This work explores a avenue to prepare heterogeneous photocatalysts to catalyze value-added reactions.

KEYWORDS: visible light, template-directed Synthesis, photocatalyst, metal-organic framework, aerobic oxidation

Utilization of visible light to promote organic transformations has drawn great attention among the past decade.[1] Photo-induced electron transfer (PET) reaction is one of the key reactions of chemical conversion of light energy, as well as synthetic organic photochemistry.[2-3] Transition metal complexes such as polypyridine ruthenium(II) complexes ($[Ru(bpy)_3]^{2+}$, bpy = 2,2'-bipyridine) were extensively employed as photocatalysts to initiate PET reactions since they possess absorption in the visible region and long excited state lifetime.[4] For instance, $[Ru(bpy)_3]Cl_2$ was used by MacMillan *et al.* as photocatalysts for the aldehyde substitution reaction in 2008,[5] and its application was later expanded to enone [2+2] cycloaddition,[6a] reductive dehalogenation of alkyl halides,[6b], and amine α-functionalization.[6c] However, most of photocatalysts used in these studies are homogeneous, which unavoidably face the drawback of traditional homogenous catalysts such as short life time, hard to recycle, environmentally unfriendly. Thus, how to make efficient heterogeneous photocatalysts to reduce the high cost, energy consumption and environmental pollution is a campaign of the field.

Immobilization homogenous catalysts into porous solid supports has been proved to be a feasible strategy to prepare heterogeneous catalysts. In the past two decades, metal-organic frameworks (MOFs) have emerged as a new class of crystalline porous solids with superior advantages that surpass traditional porous materials (e.g. zeolites, activated carbons, mesoporous silica) such as highest porosity, great structure versatility, tunable pore size, and readily tailored functionality.[7-9] These advantages offer MOFs great potential for applications as diverse as gas separation,[10] gas storage,[11-12] catalysis[13-16] etc.[17-20] Although many MOF-based photocatalysts have been reported, most of them were focused upon non-visible-light catalysis and did not involve organic catalysis.[21-23] There are only a few successful examples to employ MOFs as photocatalysts to catalyze organic

reactions, and most related studies have focused on covalently grafting photocatalytic moieties such as $[Ru(bpy)_3]^{2+}$ on the ligands via post-synthetic modification or diffusion method.[24-30] For instance, Cohen's group reported a MOF analogue of UiO-67 which covalently grafted $[Ru(bpy)_3]^{2+}$ moieties to effectively catalyze the oxidation of aryl boric acid.[31] Lin and co-workers incorporated $[Ru(bpy)_3]^{2+}$ species on a zirconium MOF to catalyze visible-light-driven proton reduction reaction.[32] Currently, encapsulating $[Ru(bpy)_3]^{2+}$ cations into MOFs' cavities to form catalytic $Ru(bpy)_3$@MOFs (@ = encapsulating) remains underexplored.[33-34] Template-directed synthesis method has been proved to be an efficient and powerful tool to afford control over both the structure and functionality (e.g. catalytic activity, chirality or fluorescence) of MOFs.[35-36] For example, if catalysts can serve as templates and remain present after synthesis of the MOFs, i.e. ''catalyst@MOFs'', the catalytic activity can be transferred from the templates to the formed catalyst@MOFs (Figure 1a). The pores of MOFs would allow effectively disperse the encapsulated catalysts and facilitate the transport of reactants and products, which could result in high catalytic activity. Moreover, MOFs can provide confined space and protection to the encapsulated catalysts. Our group have long focus on explore the generality of template-directed synthesis method to discover new functional MOFs. For example, we have used catalytic metalloporphyrins as templates to create a series of novel porphyrin@MOFs.[37] We found that porphyrins can template the formation of new MOFs structures which cannot be accessed by other synthesis methods, and the formed porphyrin@MOFs can efficiently catalyze epoxidation reactions of alkene.

Herein, we developed a new approach to prepare heterogeneous photocatalyst@MOFs using homogenous photocatalysts as structure-directing agents. Interestingly, using Ru or Ir photoactive moieties as templates, we were able to obtain a series of porous zeolite-like MOFs with sodalite-type cages. Moreover, in some MOF example, we can precisely determine the encapsulated $[Ru(bpy)_3]^{2+}$ moieties without any disorder, which greatly facilitate the understanding the guest-host interaction and the templating mechanism. These photocatalyst@MOFs possess high robustness and porosity, and can efficiently catalyze the reaction of aerobic oxidation of benzyl halides under visible light. Compared with homogeneous catalyst, these materials showed improved catalytic activity and good reusability.

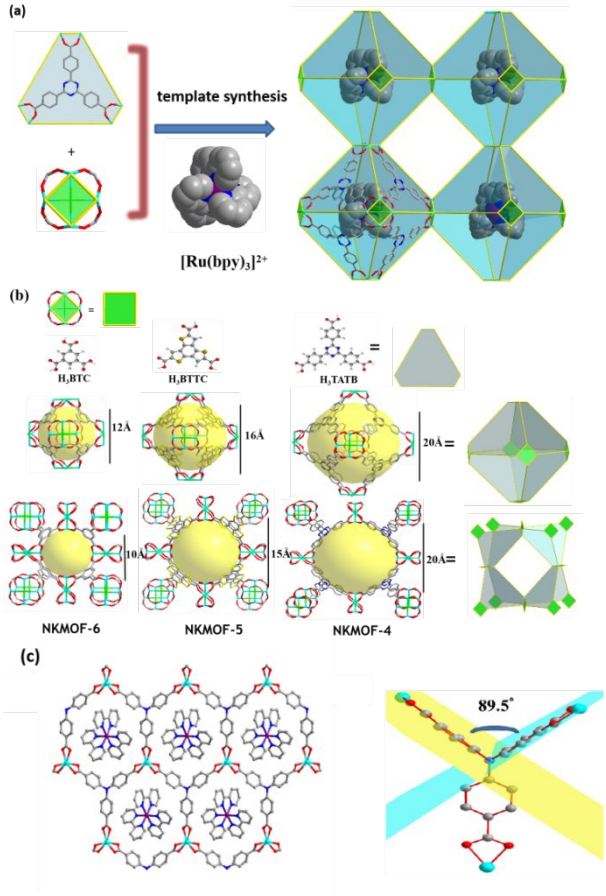

Figure 1. (a) Illumination of the template-directed synthesis strategy to prepare photocatalyst encapsulating zeolite-like MOFs. (b) The sodalite-like cage consisted of 8 hexagons and 6 squares and open channels surrounded by four sodalite-like cages. (c) The 2D layer structure of **$Ru(bpy)_3$@NKMOF-7** with ordered $[Ru(bpy)_3]^{2+}$ located in the honeycomb cavity, and the structure illumination of NBA^{3-}.

Zeolite-like MOFs have attracted great attention owing to their confined spaces and polyhedral-cage-based structures, which offer potential for application as diverse as shape- or size-selective catalysts, ion exchangers, adsorbents (gas separation/storage).[38] Exploring new zeolite-like MOFs for catalysis applications is a campaign in the field. For the first time, we used $Ru(bpy)_3Cl_2$ as templates and rigid tricarboxylate as ligands to prepare a series of $Ru(bpy)_3$@MOFs with $[Ru(bpy)_3]^{2+}$ moieties encapsulating in the sodalite-type cages (Figure 1b). Taking H_3TATB (2,4,6-tri(4-carboxyphenyl)-1,3,5-triazine) as a representative, the reaction of $CuCl_2{\cdot}2H_2O$ with H_3TATB and $Ru(bpy)_3Cl_2$ in mixed solvent of DMF/ethanol/water at 105 °C for 2 days afforded red cubic crystals (Figure S1) of **$Ru(bpy)_3$@NKMOF-4.** By contrast, the same synthesis reaction without adding $[Ru(bpy)_3]Cl_2$ afforded different product (Figure S2), indicative of its template effect. To the best of our knowledge, **NKMOF-4** has not been reported yet. These results indicated template-directing synthesis can

generate new MOF structures which cannot be accessed by other methods. Single-crystal X-ray determination (SCXRD) revealed that **NKMOF-4** exhibited a two-fold interpenetrating framework crystallized in the cubic space group *Im*-3*m*. In this structure, Cu atoms are five-coordinated in square-pyramidal coordination geometry finished by four carboxylate oxygen atoms and a chlorine. Four crystalographically equivalent Cu atoms formed a molecular building block (MBB) of chloride-centered square-planar $[Cu_4(COO)_8Cl]^-$. A supramolecular building block (SBB) of sodalite (SOD) cage with an inner sphere space of diameter ~20 Å was formed via linking six $[Cu_4(COO)_8Cl]^-$ squares with eight planar $TATB^{3-}$ ligands. A cubic packing of these sodalite cages via sharing the $[Cu_4(COO)_8Cl]^-$ squares further extended the structure into a three-dimensional (3D) anionic framework with intersected channels (Figure 1b) with diameter ~20 Å. Interestingly, the intersected channels are large enough to accommodate another set of 3D anionic framework, thereby forming a two-fold interpenetrating structure (Figure S3). Disordered $[Ru(bpy)_3]^{2+}$ and $[(CH_3]_2NH_2]^+$ cations in the cavities serve as counterions to balance the anionic framework.

To explore the generality of this template-directed synthesis approach, we further studied two short planer tricarboxylate ligands (H_3BTTC = benzo-tris-thiophene carboxylic acid; H_3BTC = trimesic acid) with the same symmetry and molecular shape as H_3TATB. We successfully obtained **Ru(bpy)$_3$@NKMOF-5** and **Ru(bpy)$_3$@NKMOF-6** which possessed the isostructural network as **NKMOF-4.** Noteworthily, the same synthesis reaction as **Ru(bpy)$_3$@NKMOF-5** without adding $[Ru(bpy)_3]Cl_2$ afforded different product (Figure S4), indicative of the template effect of $[Ru(bpy)_3]Cl_2$. By contrast, **NKMOF-6** can be obtained without adding $[Ru(bpy)_3]Cl_2$ as template[39] (Figure S5). In addition, because the sizes of sodalite cage (16 Å for **Ru(bpy)$_3$@NKMOF-5**, 12 Å for **Ru(bpy)$_3$@NKMOF-4**) are larger than the channel sizes (15 Å and 10 Å for **Ru(bpy)$_3$@NKMOF-5** and **-4,** respectively), there is no structural interpenetration observed for **NKMOF-5** and **NKMOF-4**. Due to the lack of long-range orderness of encapsulated $[Ru(bpy)_3]^{2+}$ moieties, we cannot fully determine the position of $[Ru(bpy)_3]^{2+}$ in **NKMOF-4**, **-5** and **-6**. However, based on the electron density maps, we observed $[Ru(bpy)_3]^{2+}$ cations trapped in the sodalite cages (Figure S6).

In order to further understand the reason H_3TATB, H_3BTTC and H_3BTC form the same structure with sodalite cages, we chose a non-planar ligand (H_3NBA = 4,4',4''-nitrilotribenzoic acid) as comparison. In H_3NBA, both the phenyl rings and carboxylic groups are not on the same plane and with a large distortion angle ~89^o (Figure 1c), while all atoms in H_3TATB, H_3BTTC and H_3BTC possess good coplanarity. Interestingly, the reaction of Cu^{2+} salt with H_3NBA and $Ru(bpy)_3Cl_2$ afforded red sheet-like crystals (Figure S1) of **Ru(bpy)$_3$@NKMOF-7** which crystallized in the trigonal space group of *P*312. On the contrary, the same synthesis reaction without adding $[Ru(bpy)_3]Cl_2$ afforded a clear solution (Figure S7), indicative of the template effect of $[Ru(bpy)_3]Cl_2$. In **Ru(bpy)$_3$@NKMOF-7**, there is only one crystalographically equivalent Cu atom, which is 6-coordinated with six carboxylate oxygens. The 3-connected $[Cu(COO)_3]^-$ MBBs can link with the 3-connected NBA^{3-} ligands to produce a two-dimensional (2D) honeycomb net with **hcb** topology. These 2D honeycomb nets further packed into a 3D supramolecular structure via an ABA packing mode (Figure S8). Notably, $[Ru(bpy)_3]^{2+}$ cations can be precisely determined in the cavity of the honeycomb net to balance the charge from anionic framework (Figure 1c). Notably, we found no structural distortion for $Ru(bpy)_3$ in **Ru(bpy)$_3$@NKMOF-7**. The well-defined position and full occupancy of $[Ru(bpy)_3]^{2+}$ cations in **Ru(bpy)$_3$@NKMOF-7** can help to predict the position of $[Ru(bpy)_3]^{2+}$ cations in other $Ru(bpy)_3$@MOFs. Based on these results, we concluded that the coplanarity and C_3 symmetry of ligands play key roles to generate the sodalite-like structures.

One attractive advantage of zeolite-like MOFs is their high structural stability. Thermogravimetric analysis (Figure S9-12) together with powder X-ray diffraction (PXRD) revealed that **Ru(bpy)$_3$@NKMOF-4**, **-5** and **-6** exhibited excellent thermal stability. **Ru(bpy)$_3$@NKMOF-4, -5** and **-6** can maintain their crystallinity up to 220 °C heating (Figure S13-S15). In addition, we found $Ru(bpy)_3$@NKMOFs were stable in various solvents, which are essential for catalysis application (Figure S16-19). To evaluate the porosity of $Ru(bpy)_3$@NKMOFs, N_2 sorption isotherms were then collected at 77 K. $Ru(bpy)_3$@NKMOFs were pre-exchanged with methanol and then activated via a supercritical CO_2 drying method. N_2 sorption revealed that **Ru(bpy)$_3$@NKMOF-4**, **-5** and **-6** possess BET and Langmuir surface areas of 805 m^2/g and 965 m^2/g, 1481 m^2/g and 1882 m^2/g, 480 m^2/g and 588 m^2/g, respectively (Figure S20, Table S2). Due to the pore blockage of $[Ru(bpy)_3]^{2+}$ counterions, no N_2 adsorption was observed for **Ru(bpy)$_3$@NKMOF-7**, indicative of its nonporous nature. The pore size distribution calculated on N_2 sorption isotherms revealed that **Ru(bpy)$_3$@NKMOF-4**, **-5** and **-6** possessed pore sizes centered around 9 Å, 12 Å and 8 Å, respectively (Figure S20), which are large enough to accommodate catalysis substrates (Table S3 and S4). ICP-OES (Inductively coupled plasma - optical emission spectrometry) analysis showed 60%, 52%, 42% and 100% $[Ru(bpy)_3]^{2+}$ loading for **Ru(bpy)$_3$@NKMOF-4**, **-5, -6,** and **-7**, respectively (100% loading: the anionic framework is fully balanced

by $[Ru(bpy)_3]^{2+}$ cations without $[(CH_3)_2NH_2]^+$). Scanning electron microscope (SEM) and energy dispersive spectrometry (EDS) further proved the uniform dispersion of Ru species (Figure S21-24) in all $Ru(bpy)_3$@NKMOFs. H^1 NMR data of digested $Ru(bpy)_3$@NKMOFs also proved the existence of 2,2'-bipyridine moieties from $[Ru(bpy)_3]^{2+}$ (Figure S25-28).

The open channels or polyhedral cages of MOFs would allow effectively disperse the photocatalyst and facilitate the transport of reactants and products, which could bring high activity in catalytic reactions. Hence, the catalytic activity of $Ru(bpy)_3$@NKMOFs were examined by two model reactions, aerobic oxidation of benzyl halides[40] and the cyclization of tertiary anilines and maleimides[41] under visible light irradiation. Both reactions are important organic reactions which have not been studied in MOF materials yet. **$Ru(bpy)_3$@NKMOF-4** was selected to be a representative to optimize these reaction conditions. These two reactions can utilize oxygen in the air and belong to typical resource-saving oxidation reactions. The UV-Vis absorption of **$Ru(bpy)_3$@NKMOF-4** showed a strong broad absorption peak in 400-600 nm, thus we selected a compact fluorescent lamp (CFL) as light source for these reactions.

Table 1. Optimization of reaction condition of aerobic oxidation of benzyl halide.[a]

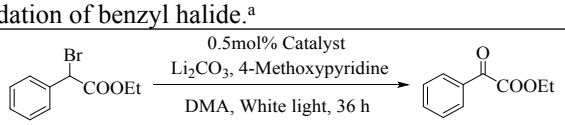

1a 2a

Entry	Catalyst	Base	Solvent	Yield[b] (%)
1	**$Ru(bpy)_3$@NKMOF-4**	Li_2CO_3	DCM	67
2	**$Ru(bpy)_3$@NKMOF-4**	Li_2CO_3	Toluene	trace
3	**$Ru(bpy)_3$@NKMOF-4**	Li_2CO_3	DMF	76
4	**$Ru(bpy)_3$@NKMOF-4**	Li_2CO_3	MeCN	89
5	**$Ru(bpy)_3$@NKMOF-4**	Li_2CO_3	DMA	96
6	**$Ru(bpy)_3$@NKMOF-4**	Pyridine	DMA	75[d]
7	**$Ru(bpy)_3$@NKMOF-4**	Na_2CO_3	DMA	62
8	**$Ru(bpy)_3$@NKMOF-4**	Li_2CO_3	DMA	50[e]
9	**$Ru(bpy)_3$@NKMOF-4**	Li_2CO_3	DMA	Trace[f]
10	**$Ru(bpy)_3$@NKMOF-4**	Li_2CO_3	DMA	70[g]
11	**$Ru(bpy)_3$@NKMOF-7**	Li_2CO_3	DMA	35
12	**$Ru(bpy)_3$@NKMOF-6**	Li_2CO_3	DMA	94
13	**$Ru(bpy)_3$@NKMOF-5**	Li_2CO_3	DMA	86
14	None	Li_2CO_3	MeCN	Trace
15	H_3BTTC	Li_2CO_3	MeCN	Trace
16	H_3BTC	Li_2CO_3	MeCN	Trace
17	H_3TATB	Li_2CO_3	MeCN	Trace
18	$CuCl_2$	Li_2CO_3	MeCN	Trace
19	**NKMOF-6**	Li_2CO_3	MeCN	Trace
20	**HKUST-1**	Li_2CO_3	MeCN	Trace
21	$Ru(bpy)_3Cl_2$	Li_2CO_3	DMA	85
22	**NKMOF-6**+$Ru(bpy)_3Cl_2$	Li_2CO_3	DMA	86[c]
23	**UiO-67-Ru**	Li_2CO_3	DMA	67
24	**$Ru(bpy)_3$@MCM-41**	Li_2CO_3	DMA	77

[a] Reactions were performed with ethyl 2-bromo-2-phenylacetate (0.2 mmol), base (0.2 mmol), 4-Methoxypyridine (20 mol%) in the presence of catalyst (0.5 mol%) for 36 h. [b] Determined by ^1H NMR spectroscopy. [c] **NKMOF-6** and $Ru(bpy)_3Cl_2$ were added together. [d] Using 2 eq pyridine as base, in absence of cocatalyst. [e] In the presence of 10 mol% 4-Methoxypyridine. [f] Without 4-Methoxypyridine. [g] 15 W blue LEDs as light source.

For the reaction of aerobic oxidation of benzyl halide,[40] in our initial investigation, we selected ethyl 2-bromo-2-phenylacetate as the model substrate to explore the optimal reaction conditions (Table 1). The reaction was performed in the presence of **$Ru(bpy)_3$@NKMOF-4** (0.5 mol%) (mass of catalyst is calculated on the basis of the molecular formula (Table S2) and Ru loading) in DCM for 36 h. The desired oxidation product was obtained in 67% yield (Table 1, entry 1). We screened various solvents for the catalytic system (Table 1, entries 2-5) and found DMA gave the product in 96% yield (TON = 192, TOF = 5.33/h). Subsequently, we studied the influence of base to the catalytic activity of **$Ru(bpy)_3$@NKMOF-4**. We found Li_2CO_3 afforded the highest yield (96%), while other inorganic base (Na_2CO_3) and organic base (pyridine) gave diminished yields of 62% and 75%, respectively (Table 1, entry 6-7). Moreover, we found the yield was reduced to 50% when reducing the dosage of cocatalyst (4-methoxypyridine) (Table 1, entry 8), and only trace product was detected when without cocatalyst (Table 1, entry 9). Also, the yield was dropped to 70% when 15 W blue LEDs was used as light source (Table 1, entry 10). The heterogeneity of **$Ru(bpy)_3$@NKMOF-4** was verified via a hot-filtration experiment. After removal of the catalyst after reacting for 10 h (yield ~50%) reaction, no more product was detected during the next 6 h under light irradiation (Figure 2a). Subsequently, after adding **$Ru(bpy)_3$@NKMOF-4** back to the reaction system, the reaction continued and the yield reached to 96% when extending the irradiation time to another 20 h. ICP-OES result of filtrated solution after the catalytic reaction proved no leaching of catalytic species from **$Ru(bpy)_3$@NKMOF-4** into solution. Moreover, we further compared the PXRD patterns of **$Ru(bpy)_3$@NKMOF-4** before and after catalytic reaction, and found the crystallinity of **$Ru(bpy)_3$@NKMOF-4** catalyst fully retained (Figure S30). There results revealed the excellent stability of **$Ru(bpy)_3$@NKMOF-4** catalyst. To further explore the advantage of heterogeneous catalyst, we tested the reusability of **$Ru(bpy)_3$@NKMOF-4** which could be easily recovered by filtration and reused for at least 5 times without significant loss of catalytic activity (Figure 2b). All these results suggest that **$Ru(bpy)_3$@NKMOF-4** is a true heterogeneous catalyst which exhibits high robustness and good reusability.

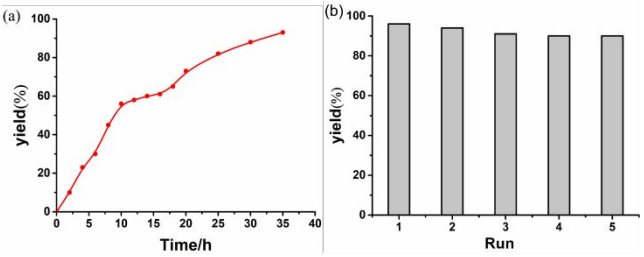

Figure 2. (a) Hot filtration experiment of **Ru(bpy)$_3$@NKMOF-4** as catalyst. Catalyst was added in the initial 0-10 h; the catalyst was removed in 10-16 h; catalyst was added back after 16 h. (b) Catalytic cycling experiment of **Ru(bpy)$_3$@NKMOF-4** as catalyst.

Photocatalytic activity of other Ru(bpy)$_3$@NKMOFs was also investigated. Firstly, we tested the solid UV-Vis spectra and found a strong broad absorption of 400-600 nm for **Ru(bpy)$_3$@NKMOF-5**, **-6** and **-7** (Figure S31-33). This allows us to utilize white light as light sources. Ethyl 2-bromo-2-phenylacetate was selected as the model substrate. Firstly, the nonporous **Ru(bpy)$_3$@NKMOF-7** was chose as a comparison, which gave rise to a very low yield of 35% (entry 11, Table 1) ascribed to the surface catalysis. By contrast, **Ru(bpy)$_3$@NKMOF-5** and **Ru(bpy)$_3$@NKMOF-6** gave yields of 86% and 94%, respectively (entries 12-13, Table 1). These results indicate that the porosity is necessary for high catalytic activity. In addition, we also studied the time-dependent catalytic activity for **Ru(bpy)$_3$@NKMOF-4**, **-5** and **-6** compared with the homogenous Ru(bpy)$_3$Cl$_2$ (Figure S34). In the initial 15 h, homogeneous Ru(bpy)$_3$Cl$_2$ catalyst showed faster and higher catalytic activity than Ru(bpy)$_3$@NKMOFs, possibly due to the faster substrate diffusion into the catalytic site of homogenous system. However, after 15 h, the catalytic efficiency of **Ru(bpy)$_3$@NKMOFs** exceeded the homogeneous catalyst, indicative of the advantage to use porous MOFs as hosts. Moreover, we further explored which parts of **Ru(bpy)$_3$@NKMOFs** contributed to the high catalytic activity. Thus, we chose no catalyst, ligands, $CuCl_2$, **NKMOF-6**, **HKUST-1** (a widely studied copper-based MOF) as controls, which all afforded trace yield (entries 14-20, Table 1). By contrast, Ru(bpy)$_3$Cl$_2$ afforded 85% yield (entry 21). Therefore, we can conclude that the catalytic activity of Ru(bpy)$_3$@NKMOFs came from the photoactive $[Ru(bpy)_3]^{2+}$ species. In addition, when directly mixing **NKMOF-6** (0.5 mol%) with Ru(bpy)$_3$Cl$_2$ (0.5 mol%), the yield was only 86% (entry 22, Table 1) equivalent to the homogeneous Ru(bpy)$_3$Cl$_2$, while **Ru(bpy)$_3$@NKMOF-6** gave a boosted yield of 94%. These results further revealed the importance and necessity to encapsulate photocatalysts in the pores of MOFs. In addition, **UiO-67-Ru**[41] which covalently grafted $[Ru(bpy)_3]^{2+}$ moieties was selected as a comparison. The yield was 67% (entry 23, Table 1), which was much lower than those of **Ru(bpy)$_3$@NKMOFs**. Moreover, we encapsulated Ru(bpy)$_3$ species into **MCM-41** via a diffusion method[42]. Although the **Ru(bpy)$_3$@MCM-41** gave a 77% yield (entry 24, Table 1), its reusability was bad because **Ru(bpy)$_3$@MCM-41** almost released all Ru(bpy)$_3$ in the first catalytic reaction cycle due to weak interaction between Ru(bpy)$_3$ species and **MCM-41**. Overall, **Ru(bpy)$_3$@NKMOFs** systems showed great advantage attributed to their facile preparation, superior catalytic activity and good reusability.

Table 2. Substrate expansion for the reaction of aerobic oxidation of benzyl halides.[a]

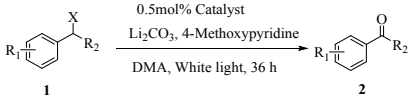

1 2

Entry	Reactants (**1**)	Products (**2**)	Yield [b] (%)
1			**2a**/96
2	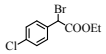	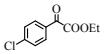	**2b**/98
3	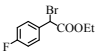	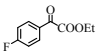	**2c**/96
4			**2d**/68
5			**2e**/73
6			**2f**/83
7			**2f**/85
8	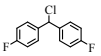	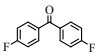	**2g**/43

[a] Reaction were performed with reactant (**1**) (0.2 mmol), Li_2CO_3 (0.2 mmol), 4-Methoxypyridine (20 mol%) in the presence of **Ru(bpy)$_3$@NKMOF-4** (0.5 mol%) in DMA (1.0 mL) for 36 h. [b] Determined by ^{1}H NMR.

With the optimal reaction conditions in hand, we then explored the reaction scope using various benzyl halides (Table 2). α-bromoarylacetic acid esters bearing various halides at the aryl ring (entries 1-5) all gave the corresponding products in good to excellent yields (68%-98%). The expansion of α-aryl carbonyl compounds to 2-halo-1,2-diphenylethanones provided good yields (83%, 85% for Table 2, entries 6, 7, respectively) as well. Although the oxidation of benzhydryl halides was not effective under the current conditions, chloride as a leaving group was tolerated in this transformation and generated the desired product in 43% yield (entries 8).

In order to further study the advantage of Ru(bpy)$_3$@NKMOFs catalysts, we used Ru(bpy)$_3$@NKMOFs to catalyze the cyclization of tertiary anilines with maleimides.[43] As shown in Table 3, substrates **3a** (0.50 mmol), **4a** (0.25 mmol), 1 mol% **Ru(bpy)$_3$@NKMOF-4** and solvent (3.0 mL) were added

into a schlenk tube. Subsequently, the reaction tube was irradiated by two 23 W compact fluorescent lamps at room temperature. We found the product **5a** was generated in 58% yield after 36 h (Table 3, entry 1) using DMF as solvent, while DCM or MeCN did not form products (entries 2-3). To further optimize the reaction conditions, we increased the amount of catalyst. When photocatalyst (**Ru(bpy)$_3$@NKMOF-4**) were increased to 2 mol% and 3 mol%, the yields increased to 73% and 93%, respectively (entries 4-5). Yield did not further improve with more catalyst loading (4 mol%, entry 6). With the optimal reaction conditions, we can obtain a good yield of 93% (TON = 31, TOF = 0.86/h) (entry 5), in contrast to the result when homogeneous Ru(bpy)$_3$Cl$_2$ (3 mol%) was applied (76%, entry 19). These results further indicated that the porosity of MOFs was necessary to the high catalytic activity. When the reaction atmosphere was changed from air to argon, the yield decreased to 18%, indicating the necessity of oxygen to the reaction (entry 7). It was found that **Ru(bpy)$_3$@NKMOF-5** and **-6** as catalysts gave yields of 83% and 89%, respectively (Table 3, entry 8-9). By contrast, the nonporous **Ru(bpy)$_3$@NKMOF-7** gave a very low yield of 32% (Table 3, entry 10), possibly attributed to the surface catalysis. To investigate which component played a key role in the catalytic process, we carried out some control experiments. It was found that the reaction did not take place without catalyst, or in the presence of the ligands or metal salts of MOFs (Table 3, entry 11-15). We also found that pure copper-based MOFs including **NKMOF-6** and **HKUST-1** cannot catalyze the reaction (entry 16-17). Moreover, when directly using a mixture of **NKMOF-6** (3 mol%) and Ru(bpy)$_3$Cl$_2$ (3 mol%), the yield was only 78% (entry 18) equivalent to the homogeneous Ru(bpy)$_3$Cl$_2$ (76%, entry 19), while **Ru(bpy)$_3$@NKMOF-6** showed a boosted yield of 89%. These results further demonstrated the advantage to encapsulate photocatalysts into porous MOFs. Additionally, we selected **UiO-67-Ru** as a comparison, and the yield was 64% (entry 20, Table 3) which was much lower than those of **Ru(bpy)$_3$@NKMOFs**.

Table 3. Optimization of reaction condition of cyclization of tertiary anilines and maleimides.[a]

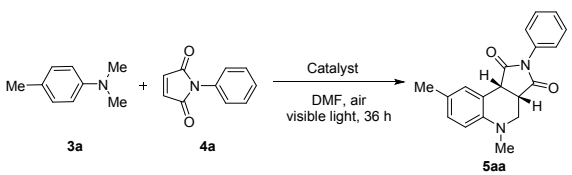

3a 4a 5aa

Entry	Catalyst	Solvent	Yield [b] (%)
1	1 mol% **Ru(bpy)$_3$@NKMOF-4**	DMF	58
2	1 mol% **Ru(bpy)$_3$@NKMOF-4**	DCM	trace
3	1 mol% **Ru(bpy)$_3$@NKMOF-4**	MeCN	trace
4	2 mol% **Ru(bpy)$_3$@NKMOF-4**	DMF	73
5	3 mol% **Ru(bpy)$_3$@NKMOF-4**	DMF	93
6	4 mol% **Ru(bpy)$_3$@NKMOF-4**	DMF	93
7	3 mol% **Ru(bpy)$_3$@NKMOF-4**	DMF	18[c]
8	3 mol% **Ru(bpy)$_3$@NKMOF-5**	DMF	83
9	3 mol% **Ru(bpy)$_3$@NKMOF-6**	DMF	89
10	3 mol% **Ru(bpy)$_3$@NKMOF-7**	DMF	32
11	None	DMF	trace
12	3 mol% H_3TATB	DMF	trace
13	3 mol% H_3BTTC	DMF	trace
14	3 mol% H_3BTC	DMF	trace
15	3 mol% $CuCl_2$	DMF	trace
16	3 mol% **NKMOF-6**	DMF	trace
17	3 mol% **HKUST-1**	DMF	trace
18	**NKMOF-6** + Ru(bpy)$_3$Cl$_2$	DMF	78
19	Ru(bpy)$_3$Cl$_2$	DMF	76
20	**UiO-67-Ru**	DMF	64

[a] Reaction condition: **3a** (0.50 mmol), **4a** (0.25 mmol), in 3.0 mL solvent and irradiation of two 23 W compact fluorescent lamps for 36 h at rt. [b] Determined by ^{1}H NMR. [c] Reaction was performed under an argon atmosphere.

A hot-filtration experiment was conducted to prove if Ru(bpy)$_3$@NKMOFs belong to heterogenous catalysts. **Ru(bpy)$_3$@NKMOF-4** with the best catalytic performance was selected as a representative. After removal of MOF catalyst after reaction for 10 h (yield 50%), there was no more product detected during the next 12 h irradiation (Figure S35a). Subsequently, after adding **Ru(bpy)$_3$@NKMOF-4** back to the reaction solution, the reaction continued and the yield can reach to 92% after further extending the irradiation time of 14 h. ICP-OES result of filtrated solution after catalysis reaction showed trace amount (<0.3%) of Ru species. These results together with the catalytic recycling experiments revealed the excellent reusability of **Ru(bpy)$_3$@NKMOF-4** (Figure S35b). We further compared the PXRD patterns of **Ru(bpy)$_3$@NKMOF-4** before and after catalytic reaction, and found its crystallinity fully retained (Figure S36). There results revealed the excellent stability of Ru catalytic species in Ru(bpy)$_3$@NKMOFs. A time-dependent catalytic activity for **Ru(bpy)$_3$@NKMOF-4** compared with the homogenous Ru(bpy)$_3$Cl$_2$ (Figure S37) further proved the superiority of our heterogeneous catalysts.

Under the optimal reaction conditions, we tested the generality of the substrates with various substituted tertiary N,N-dimethylanilines (**3**) and maleimides (**4**). As shown in Table 4, the heterogeneous catalyst showed good compatibility to broad functional groups. N-aliphatic (such as methyl, benzyl) maleimides could

generate the products **5b** and **5c** in 91% and 85% yield, respectively (entries 2-3, Table 3). In addition, we found that the electronic property of substituent groups on the aryl ring of electron-deficient olefins (**4**) can influence the reactivity. N-aryl maleimide substituted with halogen atoms afforded their corresponding tetrahydroquinolines **5d-5f** with high (83%−90%) yields (entries 4-6). N-aryl maleimide substituted with electron-donating groups such as methoxyl generated its corresponding tetrahydroquinoline **5g** in a slightly lower yield (68%, entries 7). We then shifted our attention to the scope of tertiary anilines. 4-halo (**3i, 3j**), as well as unsubstituted tertiary N,N-dimethylanilines (**3h**) could react with **4a** to form the corresponding tetrahydroquinolines (**5h-5j**) with 70%−92% yields (entries 8-10). While 3-methyl N,N-dimethylanilines (**3k**) resulted in the formation of a mixture of **5k-1** and **5k-2**, with a ratio of 1.4:1 according to ^{1}H NMR analysis. Interestingly, when **3a** (4.0 equiv) and di-N-substituted maleimides (1.0 equiv) were irradiated for 36 h under the optimized conditions, bicyclized compound **5l** were formed in 48% yield (entry 12).

Table 4. Substrate expansion of the reaction of tertiary anilines with maleimides.[a]

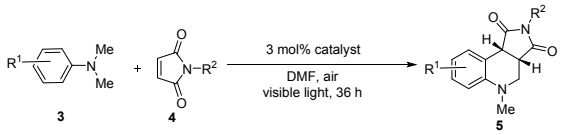

3 4 5

Entry	R^1	R^2	**5**/Yield [b] (%)
1	4-Me	Ph	**5a**/93
2	4-Me	Me	**5b**/91
3	4-Me	Bn	**5c**/85
4	4-Me	4-FPh	**5d**/90
5	4-Me	4-ClPh	**5e**/83
6	4-Me	4-BrPh	**5f**/86
7	4-Me	4-OMePh	**5g**/68
8	H	Ph	**5h**/71
9	4-F	Ph	**5i**/92
10	4-Br	Ph	**5j**/70
11	3-Me	Ph	**5k-1, 5k-2 (1.4:1)**/90
12	4-Me	di-N-substituted maleimides [c]	**5l**/48

[a] Reaction condition: tertiary N,N-dimethylanilines **3** (0.50 mmol), maleimides **4** (0.25 mmol), **Ru(bpy)$_3$@NKMOF-4** (3 mol%) in 3.0 mL solvent. [b] Determined by ^{1}H NMR. [c] The substrate used here is 1,1'-(methylenebis(4,1-phenylene))bis(1H-pyrrole-2,5-dione).

Herein, we proposed a mechanism for the catalytic of the aerobic oxidation (Scheme S1). The excited state Ru(II)* was generated under irradiation of visible light from the Ru(II) encapsulated heterogeneous photocatalyst. Pyridinium salt **I** could be generated by reaction of 4-methoxypyridine with **1a** as the literature reported. **2a** is efficiently produced from **III** with the formation of the superoxide radical anions via the alkoxyl radical intermediates **IV**. In this reaction, since MOFs did not participate in the catalytic process, we believe that the mechanism is completely consistent to the literature reports[40]. In addition, on the basis of relevant literatures[41], the mechanism for the synthesis of tetrahydroquinolines from tertiary anilines and maleimides is proposed in Scheme S2. Initially, the Ru(bpy)$_3$(II) in heterogeneous photocatalyst was irradiated to the photo-excited Ru(bpy)$_3$(II)* under visible light. Simultaneously, the single electron transfer from tertiary aniline **3a** to the photo-excited Ru(bpy)$_3$(II)* results in the generation of Ru(bpy)$_3$(I) and radical cation **A**, which is deprotonated to generate α-aminoalkyl radical **B**. Then **B** reacts with **4a** to generate intermediate **C**, which undergoes cyclization to form radical **D**. Subsequently, **D** is converted to tetrahydroquinoline **5a** by rapid oxidation of O_2. The proton eliminated from **A** is captured by HOO^- to achieve hydrogen transfer to obtain H_2O_2.

Furthermore, to illustrate the generality of this templating approach to convert homogeneous visible light catalyst into heterogeneous photocatalyst, another two commercially available homogenous photocatalysts, Ir(ppy)$_3$ (ppy = 2-phenylpyridine) and Ru(phen)$_3$Cl$_2$ (phen = 4,7-diphenyl-1,10-phenanthroline) were also used as templates (Figure S38). Two new MOF materials isomorphic with **Ru(bpy)$_3$@NKMOF-4** were obtained, named as **Ru(ph)$_3$@NKMOF-4** and **Ir(ppy)$_3$@NKMOF-4**. Their structures were further verified by SCXRD and PXRD studies data (Figure S39). ICP-OES analysis showed 20% and 8% catalyst loading, respectively. N_2 sorption data proved their permanent porosity (633 m^2/g, 564 m^2/g for **Ir(ppy)$_3$@NKMOF-4** and **Ru(phen)$_3$@NKMOF-4**, respectively) and pore size distribution (~9 Å, ~7 Å for **Ir(ppy)$_3$@NKMOF-4** and **Ru(phen)$_3$@NKMOF-4**, respectively) (Figure S40-41). Notably, we found **Ir(ppy)$_3$@NKMOF-4** and **Ru(phen)$_3$@NKMOF-4** showed better catalytic activity than **Ru(bpy)$_3$@NKMOF-4**, which is consistent with the catalysis trend of corresponding homogeneous photocatalysts. For example, for the reaction of aerobic oxidation of benzyl halide, **Ir(ppy)$_3$@NKMOF-4** and **Ru(phen)$_3$@NKMOF-4** afforded the highest yield of 99% after light irradiation for 25 h, better than the 85% yield for **Ru(bpy)$_3$@NKMOF-4** (Figure S42).

In conclusion, we developed a versatile template-directed synthesis approach to prepare new types of photocatalyst-encapsulating metal-organic frameworks (photocatalyst@MOFs) with zeolite-like structures. Due to the high robustness, permeant porosity and protection

effect of MOF matrixes, photocatalyst@MOFs showed fascinating heterogeneous catalytic activity for the reaction of aerobic oxidation of benzyl halides and the cyclization of tertiary anilines and maleimides under visible light. Interestingly, photocatalyst@MOFs exhibited boosted photocatalytic activity compared with their homogenous photocatalyst counterparts. It could be because that the pores of MOFs can effectively disperse the photocatalyst and facilitate the transport of reactants and products, which is necessary to the high catalytic activity. Moreover, we found the template-directed strategy to convert homogenous catalysts into heterogeneous systems showed high generality and can be extended to more MOF or photocatalyst systems. This research points out a new avenue to prepare highly efficient heterogeneous photocatalysts and broaden the catalytic application of MOF materials.

ASSOCIATED CONTENT

Supporting Information. Synthesis, supplementary structural figures, and supplementary characterization data, crystal data (CIF). Supporting information for this article is given via a link at the end of the document.

AUTHOR INFORMATION

Corresponding Author

pcheng@nankai.edu.cn; zhangzhenjie@nankai.edu.cn

ACKNOWLEDGMENT

The authors acknowledge the support of National Natural Science Foundation of China (21601093) and Tianjin Natural Science Foundation of China (18JCZDJC37300).

REFERENCES

(1) König, B. Photocatalysis in Organic Synthesis-Past, Present, and Future. *Eur. J. Org. Chem.* **2017**, *2017*, 1979-1981.

(2) Dadashi-Silab, S.; Doran, S.; Yagci, Y. Photoinduced Electron Transfer Reactions for Macromolecular Syntheses. *Chem. Rev*. **2016**, *116*, 10212-10275.

(3) Shaw, M. H.; Twilton, J.; MacMillan, D. W. C. Photoredox Catalysis in Organic Chemistry. *J. Org. Chem.* **2016**, *81*, 6898-6926.

(4) Juris, A.; Balzani, V.; Barigelletti, F.; Campagna, S.; Belser, P.; von Zelewsky, A. Ru(II) Polypyridine Complexes: Photophysics, Photochemistry, Eletrochemistry, and Chemiluminescence. *Coord. Chem. Rev*. **1988**, *84*, 85.

(5) Nicewicz, D. A.; MacMillan, D. W. C. Merging Photoredox Catalysis with Organocatalysis: The Direct Asymmetric Alkylation of Aldehydes. *Science* **2008**, *322*, 77-80.

(6) a) Ischay, M. A.; Anzovino, M. E.; Du, J.; Yoon, T. P. Efficient Visible Light Photocatalysis of [2+2] Enone Cycloadditions. *J. Am. Chem. Soc*. **2008**, *130*, 12886−12887.; b) Narayanam, J. M. R.; Tucker, J. W.; Stephenson, C. R. J. Electron-Transfer Photoredox Catalysis: Development of a Tin-Free Reductive Dehalogenation Reaction. *J. Am. Chem. Soc*. **2009**, *131*, 8756−8757.; c) Freeman, D. B.; Furst, L.; Condie, A. G.; Stephenson, C. R. J. Functionally Diverse Nucleophilic Trapping of Iminium Intermediates Generated Utilizing Visible Light. *Org. Lett*. **2012**, *14*, 94−97.

(7) García, H.; Navalón, S. Metal-Organic Frameworks: Applications in Separations and Catalysis. **2018**, 479-498.

(8) Lee, C. Y.; Farha, O. K.; Hong, B. J.; Sarjeant, A. A.; Nguyen, S. T.; Hupp, J. T. Light-Harvesting Metal-Organic Frameworks (MOFs): Efficient Strut-to-Strut Energy Transfer in Bodipy and Porphyrin-Based MOFs. *J. Am. Chem. Soc.* **2011**, *133,* 15858-15861.

(9) Shen, J. Q.; Liao, P. Q.; Zhou, D. D.; He, C. T.; Wu, J. X.; Zhang, W. X.; Zhang, J. P.; Chen, X. M. Modular and Stepwise Synthesis of a Hybrid Metal-Organic Framework for Efficient Electrocatalytic Oxygen Evolution. *J. Am. Chem. Soc.* **2017**, *139*, 1778-1781.

(10) Xue, M.; Zhang, Z. J.; Xiang, S. C.; Jin, Z.; Liang, C. D.; Zhu, G. S.; Qiu, S. L.; Chen, B. L. Selective Gas Adsorption within a Five-Connected Porous Metal-Organic Framework. *J. Mater. Chem.* **2010**, *20,* 3984–3988.

(11) Yang, S. H.; Lin, X.; Blake, A. J.; Walker, G. S.; Hubberstey, P.; Champness, N. R.; Schröder, M. Cation-Induced Kinetic Trapping and Enhanced Hydrogen Adsorption in a Modulated Anionic Metal-Organic Framework. *Nat. Chem*. **2009**, *1*, 487–493.

(12) Liao, Y. J.; Zhang, L.; Weston, M. H.; Morris, W.; Hupp J. T.; Farha O. K. Tuning Ethylene Gas Adsorption via Metal Node Modulation: Cu-MOF-74 for a High Ethylene Deliverable Capacity. *Chem. Commun.* **2017**, *53*, 9376–9379.

(13) Liu, J. W.; Chen, L. F.; Cui, H.; Zhang, J. Y.; Zhang, L.; Su, C. Y. Applications of Metal-Organic Frameworks in Heterogeneous Supramolecular Catalysis. *Chem. Soc. Rev.* **2014**, *43*, 6011–6061.

(14) Chughtai, A. H.; Ahmad, N.; Younus, H. A.; Laypkovc, A.; Verpoort, F. Metal-Organic Frameworks: Versatile Heterogeneous Catalysts for Efficient Catalytic Organic Transformations. *Chem. Soc. Rev.* **2015**, *44*, 6804-6849.

(15) Yoon, M.; Srirambalaji, R.; Kim, K. Homochiral Metal-Organic Frameworks for Asymmetric Heterogeneous Catalysis. *Chem. Rev.* **2012**, *112*, 1196-1231.

(16) Ma, L. Q.; Abney, C.; Lin, W. B. Enantioselective Catalysis with Homochiral Metal-Organic Frameworks. *Chem. Soc. Rev.* **2009**, *38*, 1248-1256.

(17) Lykourinou, V.; Chen, Y.; Wang, X. S.; Meng, L.; Hoang, T.; Ming, L. J.; Musselman, R. L.; Ma, S. Q. Immobilization of MP-11 into a Mesoporous Metal-Organic Framework, MP-11@mesoMOF: A New Platform for Enzymatic Catalysis. *J. Am. Chem. Soc.* **2011**, *133*, 10382-10385.

(18) An, J.; Geib, S. J.; Rosi, N. L. Cation-Triggered Drug Release from a Porous Zinc-Adeninate Metal-Organic Framework. *J. Am. Chem. Soc.* **2009**, *131*, 8376-8377.

(19) Horcajada, P.; Serre, C.; Vallet-Regi, M.; Sebban, M.; Taulelle, F.; Férey, G. Metal-Organic Frameworks as Efficient Materials for Drug Delivery. *Angew. Chem. Int. Ed.* **2006**, *45*, 5974-5978.

(20) Martell, J. D.; Porter-Zasada, L. B.; Forse, A. C.; Siegelman, R. L.; Gonzalez, M. I.; Oktawiec, J.; Runčevski, T.; Xu, J. W.; Srebro-Hooper, M.; Milner, P. J.; Colwell, K. A.; Autschbach, J.; Reimer, J. A.; Long, J. R. Enantioselective Recognition of Ammonium Carbamates in a Chiral Metal-Organic Framework. *J. Am. Chem. Soc.* **2017**, *139*, 16000-16012.

(21) Xiao, J. D.; Jiang, H. L. Metal-Organic Frameworks for Photocatalysis and Photothermal Catalysis. *Acc. Chem. Res.* **2019**, *52*, 356-366.

(22) Zeng, L; Guo, X. Y.; He C, Duan, C. Y. Metal-Organic Frameworks: Versatile Materials for Heterogeneous Photocatalysis. *ACS Catal.* **2016**, *6*, 7935-7947.

(23) Jiao, L.; Wang, Y.; Jiang H. L.; Xu, Q. Metal-Organic Frameworks as Platforms for Catalytic Applications. *Adv. Mater*. **2018**, *30,* 1703663.

(24) Liu, Y. Y.; Moon, S. Y.; Hupp, J. T.; Farha, O. K. Dual-Function MetalOrganic Framework as a Versatile Catalyst for Detoxifying Chemical Warfare Agent Simulants. *ACS Nano.* **2015**, *9*, 12358-12364.

(25) Wang, C.; deKrafft, K. E.; Lin, W. B. Pt Nanoparticles@Photoactive Metal-Organic Frameworks: Efficient Hydrogen Evolution via Synergistic Photoexcitation and Electron Injection. *J. Am. Chem. Soc.* **2012**, *134*, 7211-7214.

(26) Canivet, J.; Aguado, S.; Schuurman, Y.; Farrusseng, D. MOF-Supported Selective Ethylene Dimerization Single-Site Catalysts

through One-Pot Postsynthetic Modification. *J. Am. Chem. Soc.* **2013**, *135,* 4195-4198.

(27) Shi, D. Y.; He, C.; Qi, B.; Chen, C.; Niub, J. Y.; Duan, C. Y. Merging of the Photocatalysis and Copper Catalysis in Metal–Organic Frameworks for Oxidative C–C Bond Formation. *Chem. Sci.,* **2015**, *6,* 1035-1042.

(28) Pintado-Sierra, M.; Rasero-Almansa, A. M.; Corma, A.; Iglesias, M.; Sánchez, F. Bifunctional Iridium-(2-aminoterephthalate)–Zr-MOF Chemoselective Catalyst for the Synthesis of Secondary Amines by One-pot Three-step Cascade Reaction. *J. Catal.* **2013**, *299,* 137-145.

(29) Wang, C.; Xie, Z. G.; Dekrafft, K. E.; Lin, W. B. Doping Metal-Organic Frameworks for Water Oxidation, Carbon Dioxide Reduction, and Organic Photocatalysis. *J. Am. Chem. Soc.* **2011**, *133*, 13445-13454.

(30) Maza, W. A.; Haring, A. J.; Ahrenholtz, S. R.; Epley, C. C.; Lin, S. Y.; Morris, A. J. Ruthenium(II)-Polypyridyl Zirconium(IV) Metal-Organic Frameworks as a New Class of Sensitized Solar Cells. *Chem. Sci.* **2016**, *7*, 719-727.

(31) Yu, X.; Cohen, S. M. Photocatalytic Metal-Organic Frameworks for the Aerobic Oxidation of Arylboronic Acids. *Chem. Commun.* **2015**, *51*, 9880-9883.

(32) Zhang, Z. M.; Zhang, T.; Wang, C.; Lin, Z. K.; Long, L. S.; Lin, W. B. Photosensitizing Metal-Organic Framework Enabling Visible-Light-Driven Proton Reduction by a Wells-Dawson-Type Polyoxometalate. *J. Am. Chem. Soc.* **2015**, *137*, 3197-3200.

(33) Whittington, C. L.; Wojtas, L.; Larsen, R. W. Ruthenium(II) Tris(2,2-bipyridine)-Templated Zinc(II) 1,3,5-Tris(4-carboxyphenyl)benzene Metal Organic Frameworks: Structural Characterization and Photophysical Properties. *Inorg. Chem.* **2014**, *53,* 160-166.

(34) Wang, X.; Lu, W.; Gu, Z.-Y.; Wei, Z.; Zhou, H.-C. Topology-guided Design of an Anionic Bor-Network for Photocatalytic $[Ru(bpy)_3]^{2+}$ Encapsulation. *Chem. Commun.* **2016**, *52*, 1926-1929.

(35) Shi, Q.; Xu, W. J.; Huang, R. K.; Zhang, W. X.; Li, Y.; Wang, P. F.; Shi, F. N.; Li, L. B.; Li, J. P.; Dong, J. X. Zeolite CAN and AFI-Type Zeolitic Imidazolate Frameworks with Large 12-Membered Ring Pore Openings Synthesized Using Bulky Amides as Structure-Directing Agents. *J. Am. Chem. Soc.* **2016**, *138*, 16232-16235.

(36) Guo, X.; Geng, S.; Sun, J. Zaworotko, M. J.; Chen, Y.; Cheng, P.; Zhang, Z. The Utility of the Template Effect in Metal-Organic Frameworks. *Coord. Chem. Rev.* **2019**, *391,* 44-68.

(37) Zhang, Z. J.; Zhang, L.; Lukasz, W.; Nugent, P.; Eddaoudi, M.; Zaworotko, M, J. Templated Synthesis, Postsynthetic Metal Exchange, and Properties of a Porphyrin-Encapsulating Metal–Organic Material. *J. Am. Chem. Soc.* **2011**, *134*, 924-927.

(38) Eddaoudi, M.; Sava, D. F.; Eubank, J. F.; Adila, K.; Guillerm, V. Zeolite-Like Metal-Organic Frameworks (ZMOFs): Design, Synthesis, and Properties. *Chem. Soc. Rev.,* **2015**, *44*, 228-249.

(39) Tan, Y. X.; He, Y. P.; Zhang, J. Pore Partition Effect on Gas Sorption Properties of an Anionic Metal-Organic Framework with Exposed Cu^{2+} Coordination Sites. *Chem. Commun*. **2011**, *47*, 10647-10649.

(40) Su, Y. J.; Zhang, L. R.; Jiao, N. Utilization of Natural Sunlight and Air in the Aerobic Oxidation of Benzyl Halides. *Org. Lett.* **2011**, *13*, 2168-2171.

(41) Maza, W. A.; Morris. A. J. Photophysical Characterization of a Ruthenium(II) Tris(2,2′-Bipyridine)-Doped Zirconium UiO-67 Metal-Organic Framework. *J. Phys. Chem. C* **2014**, *118*, 8803-8817.

(42) Bottinelli, E.; Miletto, I.; Caputo, G.; Coluccia, S.; Gianotti, E. Photoactive Ru Complex Embedded in Mesostructured MCM-41 Nanoparticles. J. Fluoresc. **2011**, *21*, 901-909.

(43) Ju, X. H.; Li, D. J.; Li, W. F,; Yu, W.; Bian, F. L. The Reaction of Tertiary Anilines with Maleimides under Visible Light Redox Catalysis. *Adv. Synth. Catal.* **2012**, *354*, 3561-3567.

Table of Contents artwork: